ELSEVIER

Journal of Nuclear Materials 280 (2000) 25–32

journal of nuclear materials

www.elsevier.nl/locate/jnucmat

Studies on the kinetics of oxidation of urania–thoria solid solutions in air

S. Anthonysamy [a], Kitheri Joseph [b], T. Gnanasekaran [b], P.R. Vasudeva Rao [a,*]

[a] *Fuel Chemistry Division, Indira Gandhi Centre for Atomic Research, Kalpakkam 603 102, India*
[b] *Materials Chemistry Division, Indira Gandhi Centre for Atomic Research, Kalpakkam 603 102, India*

Received 10 September 1999; accepted 6 March 2000

Abstract

The oxidation behaviour of $(U_yTh_{1-y})O_2$ powders ($y = 0.15, 0.30, 0.72$ and 0.77) was studied by means of thermogravimetry. The oxidation was carried out under both isothermal and non-isothermal conditions. The limits of oxygen solubility in terms of O/M ratios of $(U_yTh_{1-y})O_2$ solid solutions, derived from the thermogravimetric data, were 2.08, 2.15, 2.35 and 2.36 for $y = 0.15, 0.30, 0.72$ and 0.77, respectively. A single-step oxidation was observed for $(U_yTh_{1-y})O_2$ solid solutions with $y = 0.15$–0.77. The activation energy for the oxidation of $(U_yTh_{1-y})O_2$ powders with $y = 0.15$ and 0.30 (the final product is single-phase), was found to be (48.5 ± 2.5) kJ mol^{-1}. The activation energy for the oxidation of $(U_yTh_{1-y})O_2$ powders with $y = 0.72$ and 0.77 (the final product is a bi-phasic mixture) was found to be (86.5 ± 4.5) kJ mol^{-1}.

1. Introduction

$(U,Th)O_2$ and $(Pu,Th)O_2$ solid solutions are considered as potential fuels for advanced thermal reactors [1–3]. Investigations on the oxidation behaviour of these materials are not only useful in understanding the nature of the oxidation process to establish its mechanism but also of relevance in their industrial applications as nuclear fuels. Recently Sali et al. [4] have studied the kinetics of oxidation of $(Pu_yTh_{1-y})O_{2-x}$ ($y = 0.2$, 0.3 and 0.7) pellets in air by thermogravimetry in the temperature range 400–1200 K. However, the kinetics of oxidation of $(U,Th)O_2$ powders have not been reported in the literature, although the oxidation behaviour and the limits of oxygen solubility in the UO_2–ThO_2 system have been communicated [5–8].

New methods, based on microwave combustion synthesis (commonly known as self-propagating high temperature synthesis), are being developed at our Centre with the objective of preparing ThO_2 as well as $(U,Th)O_2$ powder feed capable of yielding fine grained high density pellets at relatively low sintering temperatures [9–11]. It will be of interest to investigate the nature of oxidation of $(U,Th)O_2$ powders obtained from these pellets. In the present study, the kinetics of oxidation of $(U_{0.15}Th_{0.85})O_2$ and $(U_{0.30}Th_{0.70})O_2$ (low-urania solid solutions) and $(U_{0.72}Th_{0.28})O_2$ and $(U_{0.77}Th_{0.23})O_2$ (high-urania solid solutions) powders were examined by means of thermogravimetry. The mechanism of the oxidation process was determined from the analysis of thermogravimetric data. The kinetic parameters of the oxidation process are reported in this study for the first time.

2. Experimental

2.1. Chemicals

Nuclear grade uranium dioxide (99.99%) was obtained from Nuclear Fuel Complex, India and thorium nitrate was from Indian Rare Earths, India. Citric acid of analytical reagent grade was from Sarabhai M. Chemicals, Mumbai, India.

* Corresponding author. Tel.: +91-4114 40 229; fax: +91-4114 40 365.
E-mail address: vasu@igcar.ernet.in (P.R. Vasudeva Rao).

0022-3115/00/$ - see front matter
PII: S0022-3115(00)00035-0

2.2. Sample preparation and characterisation

Uranyl nitrate was prepared by dissolving U_3O_8 (obtained by heating nuclear grade UO_{2+x} in air at 1073 K for 5 h) in analytical reagent grade nitric acid followed by evaporation to dryness. The aqueous solution containing uranyl nitrate, thorium nitrate and citric acid (U/(U + Th) ≈ 0.15, 0.30, 0.72, and 0.77, citric acid-to-nitrate mole ratio = 1.0) was heated using a microwave oven (frequency 2450 MHz with an output of 600–700 W) till the whole solution was converted into a powder. The product was then transferred into an alumina cup and calcined at 973 K for 5 h in air using a resistance-heating furnace in order to remove the residual carbon. The calcined powders were then compacted at 300 MPa into 10 mm diameter and 2 mm thick pellets, by employing an electrically operated double action hydraulic press, and sintered at 1573 K for 5 h in a flowing argon-2 vol.% hydrogen gas mixture whose oxygen potential was estimated to be ≈− 460 kJ mol^{-1} (flow rate: 8.3×10^{-6} m^3 s^{-1}). The density of the sintered compacts was found to be 95–96% of theoretical density. The oxygen-to-metal ratio (O/M ratio) of the compact was fixed at 2.000 by equilibrating the compact with H_2–H_2O gas mixture having an oxygen potential of −510 kJ mol^{-1} at 1073 K till equilibrium was established between the gas phase and $(U,Th)O_2$ compact. The gas equilibration assembly, the method of equilibration and the O/M measurements are described elsewhere [12]. The equilibrated compacts were then ground to powder and characterised for their chemical composition, impurity content, phase composition, specific surface area, crystallite size and particle size distribution. After the oxidation, the samples were characterised for their chemical and phase compositions.

The exact chemical composition of the starting mixed oxide was determined by both chemical characterization, involving the elemental analyses of uranium and thorium, as well as lattice parameter measurements. The details of the analytical methods employed for the elemental analyses are given in Ref. [12]. Essentially, about 200 mg of the oxides were dissolved in concentrated HNO_3 with a few drops of diluted HF. 1 ml aliquots of this solution were titrated against diethylenetriaminepentaacetic acid using xylenol orange as the indicator to determine the amount of thorium [13]. Then to the same aliquot acetic acid buffer was added to adjust the pH to 3–4. The uranium content was then determined by titrating against pyridene 2,6 dicarboxylic acid using arsenazo−1 as indicator [14].

The mixed oxide samples were analysed for their impurity content by inductively coupled plasma mass spectrometry and optical emission spectroscopy. The carbon content was determined by oxidising the sample in a stream of oxygen in an induction furnace and measuring the carbon dioxide evolved by an infrared detector.

The X-ray powder patterns were obtained using an X-ray diffractometer (XPERT MPD system obtained from Philips, The Netherlands), employing filtered Cu Kα radiation. The average crystallite size of the powders was measured by X-ray line broadening technique employing the Scherrer formula using the profiles of the (220) peak [15]. Standard silicon was used for estimation of the instrumental broadening.

The BET surface area of powders was measured using a continuous flow Nelson Eggersten type surface area analyser, Quantasorb Jr. system obtained from Quantachrome, USA. The particle size analysis was carried out with a Mastersizer particle size analyzer obtained from Malvern, Worcestershire, UK.

2.3. Experimental procedure

Simultaneous TGA-DTA measurements were carried out using a thermogravimetric analyser supplied by Rheometric Scientific, UK (Model No. STA 1500). The temperature calibration was carried out by the method of fixed melting points employing International Confederation for Thermal Analysis and Calorimetry (ICTAC) recommended standards such as indium, tin and gold. The sensitivity of the thermobalance was 1 μg in the range operated. Sintered high density alumina crucibles were used as sample holders and α-alumina powder was used as reference. About 25 mg of $(U,Th)O_2$ powder sample was used for each experiment. The powder sample was oxidised in air and measurements were carried out under isothermal and non-isothermal conditions. Experiments under non-isothermal conditions were performed at programmed heating rates of 0.5, 1, 2 and 5 K min^{-1}. In the case of isothermal runs, the specimen powders were heated at four selected temperatures corresponding to the intermediate region of the TGA curves obtained from non-isothermal runs.

3. Results

The chemical composition, lattice parameter, specific surface area, crystallite size and particle size distribution of $(U,Th)O_2$ powder samples employed in the present study are given in Table 1. The lattice parameter of the $(U,Th)O_2$ solid solution increases with increasing thorium content of the solid solution as expected from lattice parameters of stoichiometric urania and thoria. The measured values are also in agreement with the values reported in the literature [16]. The total metallic impurity in each of the mixed oxide sample employed in this study was less than 100 ppm (by weight). Hence the possibility of metallic impurities influencing the oxidation behaviour of $(U,Th)O_2$ samples can be ruled out. The amount of carbon in all samples employed in this study was found less than about 100 ppm. Since all

Table 1
The physicochemical characteristics of the samples investigated in the present study

Chemical composition	Lattice parameter (pm)	Carbon content (ppm)	Specific surface area (m^2/g)	Crystallite size (μm)	Particle size distribution in vol.%		
					10 vol.% of the sample has a particle size less than (μm)	50 vol.% of the sample has a particle size less than (μm)	90 vol.% of the sample has a particle size less than (μm)
$(U_{0.15}Th_{0.85})O_2$	557.86 ± 0.03	55	1.78	0.09	3	53	163
$(U_{0.30}Th_{0.70})O_2$	555.88 ± 0.03	65	1.64	0.10	3	48	168
$(U_{0.72}Th_{0.28})O_2$	550.72 ± 0.04	40	1.71	0.09	3	57	201
$(U_{0.77}Th_{0.23})O_2$	550.08 ± 0.04	80	1.68	0.09	1	46	150

powders had approximately the same crystallite size, surface area and particle size distribution (see Table 1), the influence of these properties on the oxidation behaviour would remain constant, and the composition of the samples alone would reflect in their differing oxidation behaviour. Reproducibility of the results obtained from different measurements was verified by carrying out measurements in duplicate or triplicate. The results were found to be in excellent agreement with each other.

3.1. Oxidation of low urania containing solid solutions

Fig. 1 shows typical simultaneous TGA and DTG curves for the oxidation of single-phase $(U_{0.15}Th_{0.85})O_2$ and $(U_{0.30}Th_{0.70})O_2$ powders at a heating rate of 5 K min^{-1} in static air. From the DTG curves it is observed that the oxidation of $(U_{0.15}Th_{0.85})O_2$ and $(U_{0.30}Th_{0.70})O_2$ occurred in a single step. XRD patterns of the oxidised products showed them to be single-phase $(U_{0.15}Th_{0.85})O_{2+p}$ and $(U_{0.30}Th_{0.70})O_{2+q}$ solid solutions (with fluorite structure) only. The values of p and q were determined from the weight gain of the samples using the following expression:

$$O/M = 2 + p(\text{or } q) = 2 + \{[M]/16\} \cdot \{\Delta W/W\},$$

where $W=$ sample weight at O/M $=$ 2.0000, $\Delta W=$ weight change relative to the stoichiometric sample weight and [M] $=$ molecular weight of $(U_yTh_{1-y})O_{2.000}$. The results are shown in Table 2. The average values of p and q were 0.07 and 0.15, respectively. Belle and Berman [16] have reviewed the measured data on the solubility of oxygen in $(U_yTh_{1-y})O_2$ as a function of the U/(U+Th) ratio. They have also computed the oxygen limit in these solid solutions by structural and electronic charge considerations. They have reported a value of 0.0743 (computed) for p and 0.159 (measured) for q. The values of p and q obtained in this study are in good agreement with the values reported by them [16].

The XRD patterns of the $(U_{0.15}Th_{0.85})O_{2+p}$ and $(U_{0.30}Th_{0.70})O_{2+q}$ solid solutions (oxidised products obtained in this study) showed a slight shift in the diffraction lines due to the inclusion of additional oxide ions in the fluorite lattice. For example, in the case of stoichiometric $(U_{0.30}Th_{0.70})O_2$, the lattice parameter was

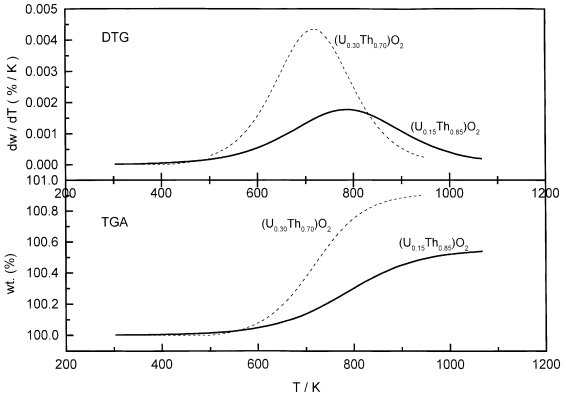

Fig. 1. TGA and DTG curves for the oxidation of $(U_yTh_{1-y})O_2$ powders with $y = 0.15$ (—) and 0.30 (– -). Heating rate is 5 K min^{-1}.

Table 2
O/M of the oxidised (U, Th)O_2 solid solutions

Composition	O/M ratio after completion of oxidation	Mean uranium valence (for the oxidised products)	Mass gain per 25 mg of the sample (in mg)
$(U_{0.15}Th_{0.85})O_2$	2.08 ± 0.01	5.06 ± 0.07	0.1208 ± 0.0075
$(U_{0.30}Th_{0.70})O_2$	2.15 ± 0.01	5.00 ± 0.03	0.2257 ± 0.0750
$(U_{0.72}Th_{0.28})O_2$	2.35 ± 0.01	4.97 ± 0.03	0.5218 ± 0.0150
$(U_{0.77}Th_{0.23})O_2$	2.36 ± 0.01	4.94 ± 0.02	0.5361 ± 0.0150

(555.88 ± 0.03) pm while that of the oxidised product with O/M = 2.15 was found to be (554.62 ± 0.04) pm. This is in agreement with the decrease in the lattice parameter when UO_2 is oxidised to UO_{2+y}, because the ionic radius of $U^{5+}$is lower than that of U^{4+}. The corresponding lattice contraction is stronger than the small dilation by interstitially dissolved excess oxygen.

3.2. Oxidation of high urania containing solid solutions

Fig. 2 shows typical TGA and DTG curves for the oxidation of single-phase $(U_{0.72}Th_{0.28})O_2$ and $(U_{0.77}Th_{0.23})O_2$ powders at a heating rate of 2 K min^{-1} in static air. It is observed from the figure that the oxidation of $(U_{0.72}Th_{0.28})O_2$ and $(U_{0.77}Th_{0.23})O_2$ also occurred in a single step. The XRD analysis of the oxidised product in each case shows them to be a biphasic mixture containing a cubic MO_{2+x} fluorite phase (M = U+Th) and an orthorhombic U_3O_8 phase, in agreement with the results reported in the literature [5–7,16]. It has been established in the literature that thoria is insoluble in U_3O_8 [17]. The O/M ratios (an average value of four measurements corresponding to four different heating rates) of the oxidised samples were determined from the weight gain of the samples and the values are shown in Table 2. The O/M values are in good agreement with the values reported by Belle and Berman [16]. The mean uranium valence, V_U, of the oxidised product, $(U_yTh_{1-y})O_{2+x}$, was computed using the expression, $V_U = 4 + 2x/y$, and these values are shown in Table 2.

3.3. Oxidation mechanism and kinetic parameters

3.3.1. Kinetics under non-isothermal conditions

TGA experimental data were used to deduce the mechanism of the oxidation reaction and to evaluate kinetic parameters. From the mass gain of the oxide sample the fraction reacted, α, was computed as a function of temperature. A typical plot of α against T (temperature) for the oxidation of $(U_yTh_{1-y})O_2$ powders ($y = 0.15$, 0.30, 0.72 and 0.77) at a heating rate of 2 K min^{-1} is shown in Fig. 3. Similar plots were obtained for other heating rates also. From these plots it is observed that, at a given heating rate, there is a systematic increase in the temperature at which the oxidation was detected (T_i) and completed (T_f), with decreasing uranium content in the solid solution. Fig. 4 shows a typical plot of α against T for the oxidation of $(U_{0.77}Th_{0.23})O_2$ powder at various heating rates. Similar plots were obtained for other compositions of the solid solutions also. As expected [18], both T_i and T_f increase systematically as heating rate increases.

The rate of the reaction under non-isothermal condition has been expressed by the following relation [19]

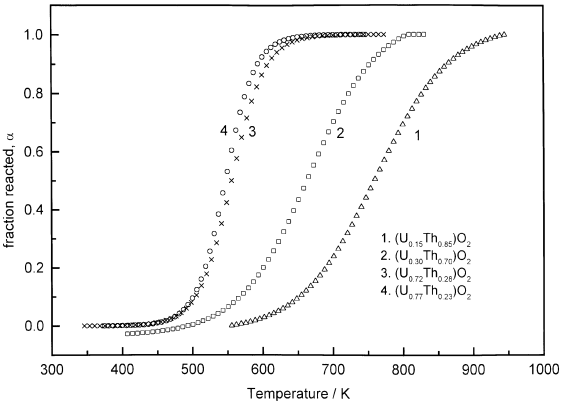

Fig. 3. α vs T plot for the oxidation of $(U_yTh_{1-y})O_2$ powders at a heating rate of 2 K min^{-1}.

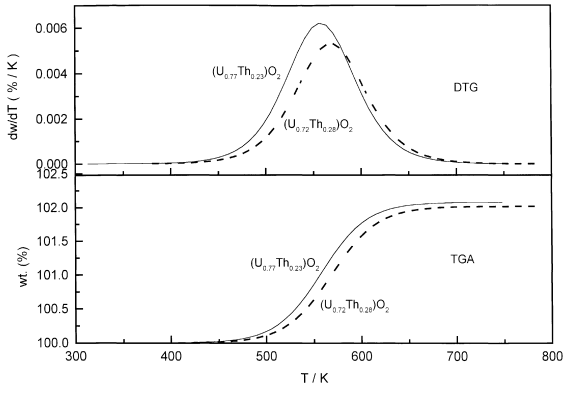

Fig. 2. TGA and DTG curves for the oxidation of $(U_yTh_{1-y})O_2$ powders with y = 0.72 (– -) and 0.77 (—). Heating rate is 2 K min^{-1}.

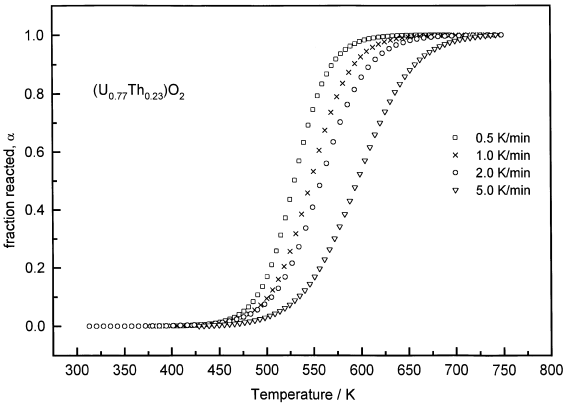

Fig. 4. α vs T plot for the oxidation of $(U_{0.77}Th_{0.23})O_2$ at various heating rates.

Table 3
List of solid state rate equations used in the present study

Rate controlling mechanism	$g(\alpha)$	References
*P*1 power law	$\alpha^{1/n}$	[26]
*E*1 exponential law	$\ln \alpha$	[19]
*A*2 Avrami–Erofe'ev equation 1	$[-\ln(1-\alpha)^{(1/2)}]$	[27–29]
*A*3 Avrami–Erofe'ev equation 2	$[-\ln(1-\alpha)]^{1/3}$	[27–29]
*A*4 Avrami–Erofe'ev equation 3	$[-\ln(1-\alpha)^{(1/4)}]$	[27–29]
*B*1 Prout–Tompkins	$\ln[\alpha/(1-\alpha)]$	[30]
*R*2 contracting area	$1-(1-\alpha)^{(1/2)}$	[19]
*R*3 contracting volume	$1-(1-\alpha)^{(1/3)}$	[19]
*D*1 one dimensional diffusion	α^2	[19]
*D*2 two dimensional diffusion	$(1\alpha)\ln(1-\alpha)+\alpha$	[19]
*D*3 three dimensional diffusion, Jander	$[1-(1-\alpha)^{(1/3)}]^2$	[31]
*D*4 three dimensional diffusion, Ginstling and Brounstein	$(1-2\alpha/3)-(1-\alpha)^{(2/3)}$	[32]
*F*1 first order	$-\ln(1-\alpha)$	[19]
*F*2 second order	$1/(1-\alpha)$	[19]
*F*3 third order	$[1/(1-\alpha)]^2$	[19]

$$\frac{d\alpha}{dT}=\frac{k(T)}{\beta}f(\alpha), \tag{1}$$

where $f(\alpha)$ is the conversion function dependent on the mechanism of the reaction, $k(T)$ is the rate constant as a function of temperature described by the Arrhenius equation $[k(T)=A\exp(-E/RT)]$ and β is the heating rate. The above equation can be represented by its integral form as

$$g(\alpha)\equiv\int_0^{\alpha}\frac{d\alpha}{f(\alpha)}=\int_0^{T}\left(\frac{A}{\beta}\right)\exp\left[-\frac{E}{RT}\right]dT, \tag{2}$$

where A is the pre-exponential factor, E the activation energy and R is the universal gas constant [20–24].

In the present study the kinetics of the oxidation was followed by applying the Coats and Redfern approximation [25]. Eq. (2) can be written as

$$\ln\left[\frac{g(\alpha)}{T^2}\right]=\ln\left[\frac{AR}{\beta E}\left(1-\frac{2RT}{E}\right)\right]-\frac{E}{RT}. \tag{3}$$

Eq. (3) is used to identify the correct form of $g(\alpha)$ to be used for the analysis of the experimental data and to obtain the most probable reaction mechanism. The algebraic expressions of $g(\alpha)$ functions for the most common mechanisms used in the kinetics of solid state reactions and tested in this work are listed in Table 3. A plot of $\ln(g(\alpha)/T^2)$ vs $1/T$ gives a straight line if the correct $g(\alpha)$ function is used in the equation. The $g(\alpha)$ function describes the mechanism of the reaction. Typical plots of $\ln(g(\alpha)/T^2)$ versus $1/T$ [where $g(\alpha)=-\ln(1-\alpha)$] for $(U_{0.15}Th_{0.85})O_2$ and $(U_{0.77}Th_{0.23})O_2$ for various heating rates are shown in Figs. 5 and 6, respectively. The corresponding kinetic parameters (activation energies and the pre-exponential factors) were derived using the Coats–Redfern equation (Eq. (3)) in the range of $\alpha=0.1$ to 0.9 for various heating rates. The results are given in Table 4.

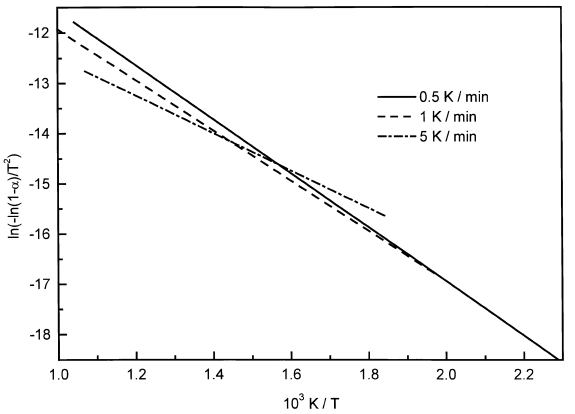

Fig. 5. $\ln(g(\alpha)/T^2)$ vs $1/T$ plot for $(U_{0.15}Th_{0.85})O_2$ at various heating rates, in the reacted fraction $\alpha=$ 0.01–0.95.

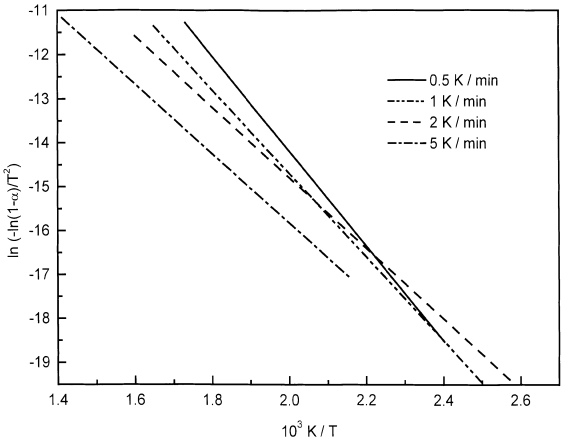

Fig. 6. $\ln(g(\alpha)/T^2)$ vs $1/T$ plot for $(U_{0.77}Th_{0.23})O_2$ at various heating rates, in the reacted fraction $\alpha=$ 0.01–0.85.

3.3.2. Kinetics under isothermal conditions

With the view to investigate the correctness of the reaction mechanism and evaluated non-isothermal kinetic parameters, isothermal experiments were carried out at four different temperatures for each composition of the solid solution. The rate of the reaction under isothermal conditions is expressed by the following relation

$$\frac{d\alpha}{dt} = f(\alpha)k(T). \tag{4}$$

The above equation can be represented by its integral form as

$$g(\alpha) \equiv \int_0^{\alpha} \frac{d\alpha}{f(\alpha)} = \int_0^{t} k(T)dt \tag{5}$$

or

$$g(\alpha) = kt. \tag{6}$$

Table 4
Non-isothermal kinetic parameters

Sample	Heating rate (K min^{-1})	Activation energy (kJ mol^{-1})	Pre-exponential factor (log A) (min^{-1})
$(U_{0.15}Th_{0.85})O_2$	0.5	45 ± 0.3	0.747 ± 0.006
	1	42 ± 0.3	0.693 ± 0.004
	5	31 ± 0.2	0.471 ± 0.002
$(U_{0.30}Th_{0.70})O_2$	0.5	51 ± 0.6	1.820 ± 0.095
	1	49 ± 0.5	1.800 ± 0.090
	5	49 ± 0.4	1.350 ± 0.073
$(U_{0.72}Th_{0.28})O_2$	0.5	81 ± 0.4	5.860 ± 0.910
	1	70 ± 0.6	4.750 ± 0.760
	2	70 ± 0.6	1.890 ± 0.035
	5	46 ± 0.4	0.728 ± 0.012
$(U_{0.77}Th_{0.23})O_2$	0.5	90 ± 0.6	7.250 ± 0.140
	1	79 ± 0.4	5.860 ± 0.160
	2	67 ± 0.8	4.760 ± 0.190
	5	66 ± 0.8	4.600 ± 0.160

Fig. 7(a)–(d) show plots of α against time for the oxidation of $(U_yTh_{1-y})O_2$ ($y = 0.15$, 0.30, 0.72 and 0.77) powders at various temperatures. Various forms of $g(\alpha)$ listed in Table 3 were used in Eq. (6) to identify the correct mechanism by the linear fit method. The values of the rate constant computed from Eq. (6) [where

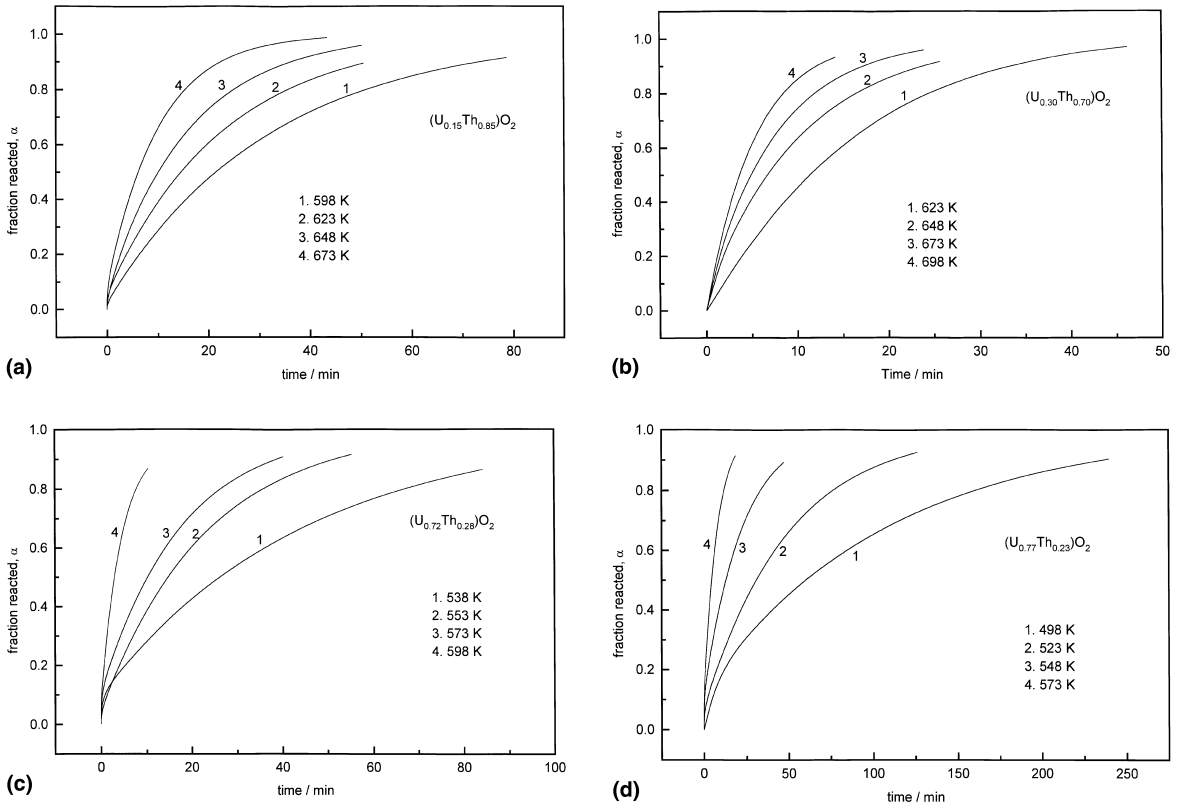

Fig. 7. Plots of α against time for the oxidation of $(U_yTh_{1-y})O_2$ powders at various temperatures (a) $y = 0.15$, (b) $y = 0.30$, (c) $y = 0.72$ and (d) $y = 0.77$.

$g(\alpha) = -\ln(1-\alpha)$] are listed in Table 5. Arrhenius plots for the oxidation of $(U_yTh_{1-y})O_2$ ($y = 0.15$, 0.30, 0.72 and 0.77) solid solutions are shown in Fig. 8. The activation energy, E, and pre-exponential factor, A, for each composition of the solid solution were evaluated using the Arrhenius equation, which are given in Table 6.

Table 5
Rate constant k as a function of temperature

Sample	Temperature (K)	k (min^{-1})
$(U_{0.15}Th_{0.85})O_2$	598	0.03094
	623	0.04337
	648	0.06139
	673	0.09823
$(U_{0.30}Th_{0.70})O_2$	623	0.07475
	648	0.09399
	673	0.13065
	698	0.18969
$(U_{0.72}Th_{0.28})O_2$	538	0.02243
	553	0.04361
	573	0.05637
	598	0.19568
$(U_{0.77}Th_{0.23})O_2$	498	0.00917
	523	0.01998
	548	0.04433
	573	0.12462

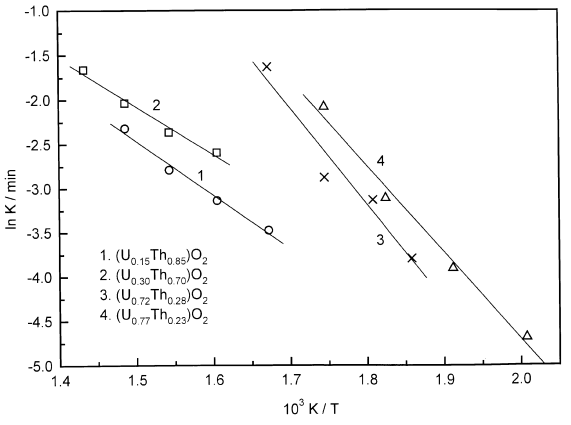

Fig. 8. Arrhenius plots for the oxidation of $(U_yTh_{1-y})O_2$ powders.

Table 6
Isothermal kinetic parameters

Sample	Activation energy E (kJ mol^{-1})	Pre-exponential factor (log A) (min^{-1})
$(U_{0.15}Th_{0.85})O_2$	51 ± 1	2.6 ± 0.4
$(U_{0.30}Th_{0.70})O_2$	45 ± 1	2.9 ± 0.3
$(U_{0.72}Th_{0.28})O_2$	91 ± 1	6.5 ± 0.6
$(U_{0.77}Th_{0.23})O_2$	82 ± 1	7.2 ± 1.4

4. Discussion

4.1. Oxidation behaviour

In the present study it has been established that the oxidation of $(U_yTh_{1-y})O_2$ solid solutions occurs in a single step irrespective of the composition of the solid solutions. Furuya [5] reported that the oxidation of $(U_yTh_{1-y})O_2$ solid solutions with $y \geqslant 0.6$ occurred in two steps corresponding to the formation of a cubic oxide of composition M_3O_7 (M = U + Th) in the first step followed by the oxidation of M_3O_7 to a biphasic mixture of cubic MO_{2+x} and orthorhombic U_3O_8 in the second step. However, the first and second stages were indistinguishable in the powders having large particle size (particle size distribution had not been reported, although the grain size in the pellet before grinding was reported to be >1 μm). In the present study, more than 50 vol.% of the powder sample had a particle size larger than approximately 50 μm and a single-step oxidation was observed for (U,Th)O_2 powders for all compositions and heating rates. It is possible that the precipitation of the orthorhombic U_3O_8 phase begins before MO_2 is completely oxidised to MO_{2+x} (single-phase) in the powder samples employed in this study and hence a single-step oxidation process is observed. The value of x in the $(U_yTh_{1-y})O_{2+x}$ fluorite phase was reported to be 0.25 when U/(U + Th) > 0.5 [16].

In general it is observed that the average O/M ratios of the oxidised (U,Th)O_2 solid solutions increase with increasing urania content in the mixed oxide. The O/M ratios of the completely oxidised products correspond to the mean valence of approximately 5 for uranium (see Table 2). These observations agree with the results obtained by Furuya [5] as well as Anderson [33].

4.2. Mechanism of oxidation

In the present study, the non-isothermal kinetics was evaluated by a model dependent method employing the Coats and Redfern approximation [25]. Model dependent methods are being extensively used to obtain reliable kinetic parameters (for example Ref. [4,34–42]). In the case of the non-isothermal kinetic analysis, out of all $g(\alpha)$ functions, the best fit (with high correlation coefficient and low standard deviation) for the oxidation process was obtained using $g(\alpha) = -\ln(1-\alpha)$ (F1 model), which corresponds to a random nucleation (one nucleation per particle) mechanism. In the case of isothermal kinetic analyses, a comparison of the fit to various kinetic models for the oxidation of (U,Th)O_2 solid solutions showed best fit only with the F1 model as observed in non-isothermal kinetics. The F1 model has been reported in the literature for the oxidation of $(Pu_yTh_{1-y})O_{2-x}$ solid solutions [4] as well as other single-phase systems such as $YBa_2Cu_3O_{7-x}$ [43].

The activation energy for each composition of the solid solution derived from the isothermal kinetics was found to be in good agreement (within ± 10%) with that obtained from the non-isothermal kinetics under lowest heating rate (0.5 K min^{-1}). This confirms the correctness of the mechanism deduced from this study for the oxidation of (U,Th)O_2 solid solutions in air. The activation energies obtained in this study for the oxidation of $(U_yTh_{1-y})O_{2+x}$ solid solutions with $y > 0.5$ were found to be higher than those for the oxidation of $(U_yTh_{1-y})O_{2+x}$ solid solutions with $y < 0.5$. In the latter case, the oxidation essentially involves the entry of additional oxygen into the fluorite lattice of the mixed oxide solid solutions whereas in the former case, the oxidation involves entry of oxygen into the lattice and simultaneous segregation of various ions resulting ultimately into the two-phase formation leading to the higher activation energies observed.

5. Conclusion

Investigations carried out in this study on the oxidation behaviour of $(U_yTh_{1-y})O_2$ powders ($y = 0.15$, 0.30. 0.72 and 0.77) by means of thermogravimetry led to the following conclusions:

1. The limits of the oxygen solubility, in terms of the O/M ratio of $(U_yTh_{1-y})O_2$ solid solutions, were 2.08, 2.15, 2.35 and 2.36 for $y = 0.15$, 0.30, 0.72 and 0.77, respectively.
2. A single-step oxidation was observed for $(U_yTh_{1-y})O_2$ powders irrespective of their composition.
3. The activation energy for the oxidation of $(U_yTh_{1-y})O_2$ powders with $y = 0.15$ and 0.30 (the final product is single-phase), was found to be (48.5 ± 2.5) kJ mol^{-1}. The activation energy for the oxidation of $(U_yTh_{1-y})O_2$ powders with $y = 0.72$ and 0.77, (the final product is a two-phase mixture) was found to be (86.5 ± 4.5) kJ mol^{-1}.

References

[1] C. Ganguly, in: P. Vincenzini (Ed.), High Tech Ceramics, Elsevier, Amsterdam, 1987, p. 2887.
[2] C. Ganguly, Development of plutonium-based advanced LMFBR fuels and thoria-based PHWR fuels in India, IAEA-TECDOC-352 (1985) pp 107–127.
[3] K. Balakrishnan, C. Ganguly, Mater. Sci. Forum 48&49 (1989) 125.
[4] S.K. Sali, S. Sampath, V. Venugopal, J. Nucl. Mater. 252 (1998) 131.
[5] H. Furuya, J. Nucl. Mater. 34 (1970) 315.
[6] I. Cohen, R.M. Berman, J. Nucl. Mater. 18 (1966) 77.
[7] R. Paul, C. Keller, J. Nucl. Mater. 41 (1971) 133.
[8] T. Matsui, K. Nato, J. Nucl. Mater. 135 (1985) 149.
[9] V. Chandramouli, S. Anthonysamy, P.R. Vasudeva Rao, R. Divakar, D. Sundararaman, J. Nucl. Mater. 231 (1996) 213.
[10] V. Chandramouli, S. Anthonysamy, P.R. Vasudeva Rao, R. Divakar, D. Sundararaman, J. Nucl. Mater 254 (1998) 55.
[11] V. Chandramouli, S. Anthonysamy, P.R. Vasudeva Rao, J. Nucl. Mater. 265 (1999) 255.
[12] S. Anthonysamy, K. Nagarajan, P.R. Vasudeva Rao, J. Nucl. Mater. 247 (1997) 273.
[13] E. Celon, S. Degetto, M. Marangoni, L. Baracco, Talanta 26 (1979) 160.
[14] R. Pribil, V. Vaseley, Talanta 10 (1963) 899.
[15] H.P. Klug, L.E. Alexander, X-ray Diffraction Procedures for Polycrystalline and Amorphous Materials, Wiley, New York, 1954.
[16] J. Belle, R.M. Berman, Thorium Dioxide: Properties and Nuclear Applications, DOE/NE-0060 (1984).
[17] R. Paul, C. Keller, J. Nucl. Mater. 41 (1971) 133.
[18] A. Blazek, Thermal Analysis, Van Nostrand Reinhold, London, 1973, p. 25.
[19] M.E. Brown, D. Dollimore, A.K. Galwey, Comprehensive Chemical Kinetics, vol. 22, Elsevier, Amsterdam 1988.
[20] J.H. Sharp, G.W. Brindley, B.N.N. Achar, J. Am. Ceram. Soc. 49 (1966) 379.
[21] D. Dollimore, T.A. Evans, Y.F. Lee, F.W. Wilburn, Thermochim. Acta 188 (1991) 77.
[22] A.R. Salvador, E.G. Calvo, Thermochim. Acta 255 (1995) 155.
[23] J. Sestak, V. Satava, W.W. Wentlandt, Thermochim. Acta 7 (1973) 447.
[24] J. Zsako, J. Phys. Chem. 72 (1968) 2406.
[25] A.N. Coats, J.P. Redfern, Nature 201 (1964) 68.
[26] A. Finch, P.W.M. Jacobs, F.C. Tompkins, J. Chem. Soc. (1954) 2053.
[27] M. Avrami, J. Chem. Phys. 7 (1939) 1103.
[28] M. Avrami, J. Chem. Phys. 8 (1940) 212.
[29] M. Avrami, J. Chem. Phys. 9 (1941) 177.
[30] E.G. Prout, F.C. Tompkins, Trans. Faraday Soc. 40 (1944) 488.
[31] W. Jander, Z. Anorg. Allg. Chem. 163 (1927) 1.
[32] A.M. Ginstling, B.I. Brounshtein, Zh. Prikl. Khim. 23 (1950) 1327.
[33] J.S. Anderson, D.N. Edgington, L.E.J. Roberts, E. Wait, J. Chem. Soc. (London) 3 (1954) 3324.
[34] M.T. Aybers, J. Nucl. Mater. 252 (1998) 28.
[35] G.A. Rama Rao, S.K. Mukerjee, V.N. Vaidya, V. Venugopal, D.D. Sood, J. Nucl. Mater. 185 (1991) 131.
[36] Y. Arai, C. Sari, J.C. Spirlet, J. Nucl. Mater. 185 (1991) 159.
[37] S.K. Mukarjee, J.V. Dehadraya, V.N. Vaidya, D.D. Sood, J. Nucl. Mater. 185 (1991) 39.
[38] K. Joseph, T. Gnanasekaran, Thermochim. Acta 342 (1999) 153.
[39] Y. Suzuki, Thermochim. Acta 255 (1995) 155.
[40] A.M. Gadalla, Thermochim Acta 95 (1985).
[41] M.R. Udupa, Thermochim. Acta 95 (1985) 179.
[42] R.K. Agrawal, Thermal Anal. Rev. Abstracts 5 (1990) 1.
[43] V. Sridharan, D. Ravichandran, S. Srinivasan, S. Sivasankaran, L. Giridhar, K. Suresh, T. Nagarajan, A. Raman, J. Mater. Sci. 27 (1992) 4483.